A conserved degron containing an amphipathic helix regulates the cholesterol-mediated turnover of human squalene monooxygenase, a rate-limiting enzyme in cholesterol synthesis

Received for publication, May 7, 2017, and in revised form, September 13, 2017 Published, Papers in Press, September 27, 2017, DOI 10.1074/jbc.M117.794230

Ngee Kiat Chua[‡], Vicky Howe[‡], Nidhi Jatana[§1], Lipi Thukral[§2], and Andrew J. Brown[‡3]

From the [‡]School of Biotechnology and Biomolecular Sciences, University of New South Wales, Sydney, New South Wales 2052, Australia and the [§]Council of Scientific and Industrial Research-Institute of Genomics and Integrative Biology, Mathura Road, Sukhdev Vihar, New Delhi 110 020, India

Edited by Dennis R. Voelker

Cholesterol biosynthesis in the endoplasmic reticulum (ER) is tightly controlled by multiple mechanisms to regulate cellular cholesterol levels. Squalene monooxygenase (SM) is the second rate-limiting enzyme in cholesterol biosynthesis and is regulated both transcriptionally and post-translationally. SM undergoes cholesterol-dependent proteasomal degradation when cholesterol is in excess. The first 100 amino acids of SM (designated SM N100) are necessary for this degradative process and represent the shortest cholesterol-regulated degron identified to date. However, the fundamental intrinsic characteristics of this degron remain unknown. In this study, we performed a series of deletions, point mutations, and domain swaps to identify a 12-residue region (residues Gln-62–Leu-73), required for SM cholesterol-mediated turnover. Molecular dynamics and circular dichroism revealed an amphipathic helix within this 12-residue region. Moreover, 70% of the variation in cholesterol regulation was dependent on the hydrophobicity of this region. Of note, the earliest known Doa10 yeast degron, Deg1, also contains an amphipathic helix and exhibits 42% amino acid similarity with SM N100. Mutating SM residues Phe-35/Ser-37/Leu-65/Ile-69 into alanine, based on the key residues in Deg1, blunted SM cholesterol-mediated turnover. Taken together, our results support a model whereby the amphipathic helix in SM N100 attaches reversibly to the ER membrane depending on cholesterol levels; with excess, the helix is ejected and unravels, exposing a hydrophobic patch, which then serves as a degradation signal. Our findings shed new light on the regulation of a key cholesterol synthesis enzyme, highlighting the conservation of critical degron features from yeast to humans.

This work was supported in part by National Health and Medical Research Council Grant 1060515 and the Australian Research Council Grant DP170101178. The authors declare that they have no conflicts of interest with the contents of this article.

This article was selected as one of our Editors' Picks.

[1] Supported by a Department of Biotechnology, Government of India, Research associateship.

[2] Supported by DST-INSPIRE Faculty Grant LSBM-45.

[3] To whom correspondence should be addressed: School of Biotechnology and Biomolecular Sciences, Biological Sciences Bldg. D26, University of New South Wales, Sydney, New South Wales 2052, Australia. Tel.: 61-2-9385-2029; Fax: 61-2-9385-1483; E-mail: aj.brown@unsw.edu.au.

The regulation of the multistep cholesterol biosynthesis pathway is a key process in cholesterol homeostasis (1). Squalene monooxygenase (SM)[4] is one of two rate-limiting steps in cholesterol biosynthesis (2) and is implicated in various human diseases, including metabolic and neurological diseases (3, 4), as well as certain cancers (5, 6). Excess cholesterol accelerates the degradation of SM by the ubiquitin–proteasome system as an example of end-product inhibition (2). Through this regulatory mechanism, SM is well-placed as a key control point in the pathway to limit cholesterol synthesis and regulate cellular cholesterol levels.

Regulated turnover of proteins via the proteasome is determined by degradation signals within the proteins themselves. These intrinsic protein elements are referred to as degrons (7). We previously showed that the first 100 amino acids of SM (SM N100) represent the region responsible for its cholesterol-mediated turnover (2). Fusing SM N100 to GFP (SM N100-GFP) causes the heterologous protein to be degraded in a cholesterol-dependent manner, indicating this region is a transferable cholesterol-regulated degron (2). To date, this represents the shortest degron known to respond to cholesterol. However, the inherent elements of these 100 amino acids that permit the cholesterol-regulated turnover event remain unknown. Examining the components of this cholesterol-regulated degron is fundamental to understand how SM fulfills its function in responding to excess cholesterol and limiting cholesterol synthesis.

We recently characterized the membrane topology of SM N100 (8). Both the N and C termini are cytosolic, and a re-entrant loop spanning 24 (between residues 18 and 41) to 33 residues (between residues 11 and 43) anchors the protein to the membranes of the endoplasmic reticulum (ER) (Fig. 1*A*). Excess cholesterol induces a conformational change in SM N100, detected at residues 9, 11 and 41, bordering the ER membrane–cytosol interface of the re-entrant loop (8). We also demonstrated that membrane-associated RING finger protein 6 (MARCH6, also called TEB4) is the E3 ubiquitin ligase respon-

[4] The abbreviations used are: SM, squalene monooxygenase; CD, methyl-β-cyclodextrin; Chol/CD, cholesterol/methyl-β-cyclodextrin; ER, endoplasmic reticulum; GOAT, ghrelin *O*-acyltransferase; HHAT, hedgehog acyltransferase; LPDS, lipoprotein-deficient serum.

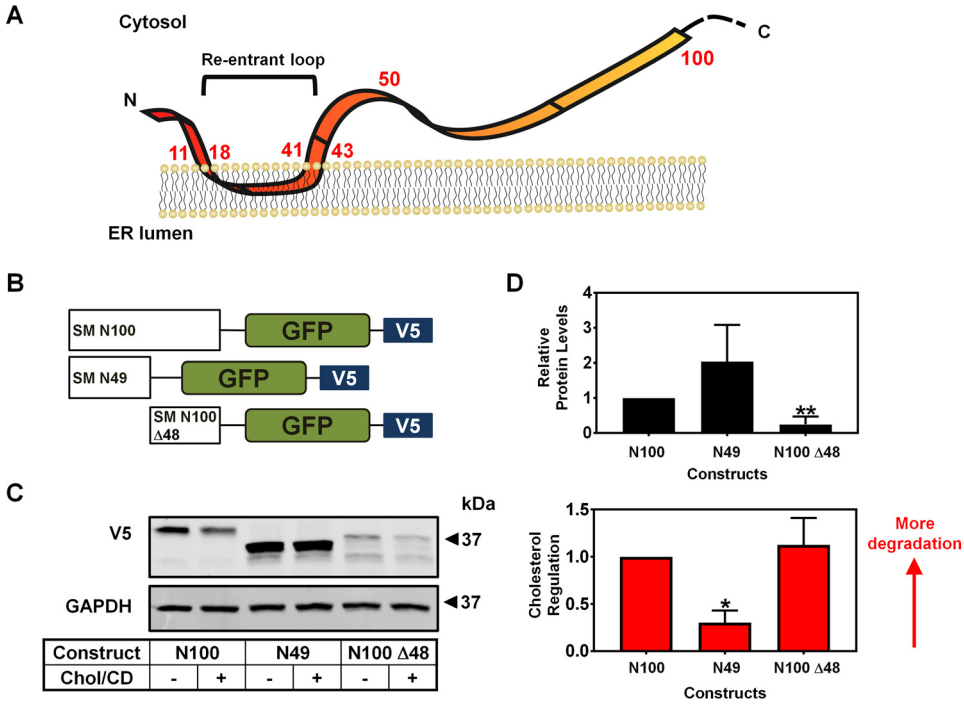

Figure 1. C-terminal half of SM N100 is required for cholesterol regulation. *A,* working model of the membrane topology of SM N100-GFP. SM N100 contains a re-entrant loop, which is embedded in the ER membrane. Residues between 11–18 and 41–43 (shown in *red*) are noted to be on the ER membrane–cytosol interface. The *black dashed lines* at the C terminus of SM N100 refer to the continuation of the protein with the linker region and GFP (not shown). The C-terminal half of SM N100 is cytosolically exposed along with GFP. *B,* schematic of truncation mutants of SM N100. All constructs contain GFP fused to the C-terminal end of SM N100 and contain a V5 epitope tag. *C,* CHO-7 cells were transfected for 24 h with the indicated SM N100 constructs (0.25 μg of expression plasmid and 0.75 μg of pTK-empty vector). Cells were then pre-treated overnight with compactin (5 μM) and mevalonate (50 μM). The next day, cells were treated for 8 h with or without Chol/CD (20 μg/ml). The Western blot is representative of at least three independent experiments. *D,* densitometric analyses of the Western blot in *C*. Data are presented as mean + S.E. from at least three independent experiments. Significant changes in cholesterol regulation or protein levels compared with WT SM N100 are indicated: *, $p \leq 0.05$, or **, $p \leq 0.01$.

sible for the cholesterol-dependent degradation of SM (9). Similarly, Erg1 is degraded by Doa10, the yeast homologs of SM and MARCH6, respectively (10). However, Erg1 lacks the critical N100 region from human SM (2), suggesting different interaction sites with the E3 ubiquitin ligase between organisms.

Doa10 targets multiple yeast substrates (10–14), including Erg1 (10) and the transcription factor Matα2 (12, 14). Matα2 contains a critical amphipathic helix region acting as a degron, termed Deg1, one of the earliest identified degrons, and has been studied extensively (12, 14). The features that define a degron are highly diverse (15). Amphipathic helices functioning as degrons have also been reported in serum and glucocorticoid-induced kinase 1 (16), Ndc10 (17), thymidylate synthase (18), and Pca1p cadmium exporter (19). In addition, the importance of intrinsically disordered regions in degrons is becoming more widely recognized (20–22).

In this study, we aimed to identify the critical regions or residues required for cholesterol regulation of SM N100, and we have discovered a key amphipathic helix located in the second half of this degron, which shares remarkable sequence homology with Deg1.

Results

C-terminal half of SM N100 expresses poorly but retains cholesterol regulation

We previously showed that the N-terminal half of SM N100 (SM N49) was not cholesterol-regulated, and we showed higher basal protein expression than SM N100 (8). Following this finding, we considered the possibility that the C-terminal half of SM N100 is critical for cholesterol regulation. We cloned the second half of SM N100 (SM N100 Δ48), fused to GFP, to test alongside the SM N49 and wild-type (WT) SM N100 constructs (Fig. 1*B*). SM N100 Δ48 protein expression was lower compared with WT SM N100 (Fig. 1, *C* and *D*), suggesting that the second half of SM N100 contains a degron element.

We also compared the cholesterol regulation of the N- and C-terminal halves of SM N100, relative to WT SM N100. We found that cholesterol regulation in SM N49 was blunted, whereas SM N100 Δ48 remained cholesterol-regulated (Fig. 1, *C* and *D*), indicating that both halves of SM N100 are required for normal cholesterol regulation and protein expression.

Cholesterol-regulated degron requires a 20-residue region in the second half of SM N100

Because cholesterol regulation was observed in the low-expressing SM N100 Δ48, and SM N49 showed blunted cholesterol regulation (Fig. 1, *C* and *D*), we predicted there was a region in the second half of SM N100 needed for cholesterol-mediated turnover. To test this, we created four constructs with successive 10-amino acid truncations of the C-terminal half of SM N100, generating SM N90, SM N80, SM N70, and SM N60, all fused to GFP (Fig. 2*A*). We tested the cholesterol regulation of these mutants and compared them with WT SM N100. Both SM N70 and SM N60 showed little to no cholesterol regulation

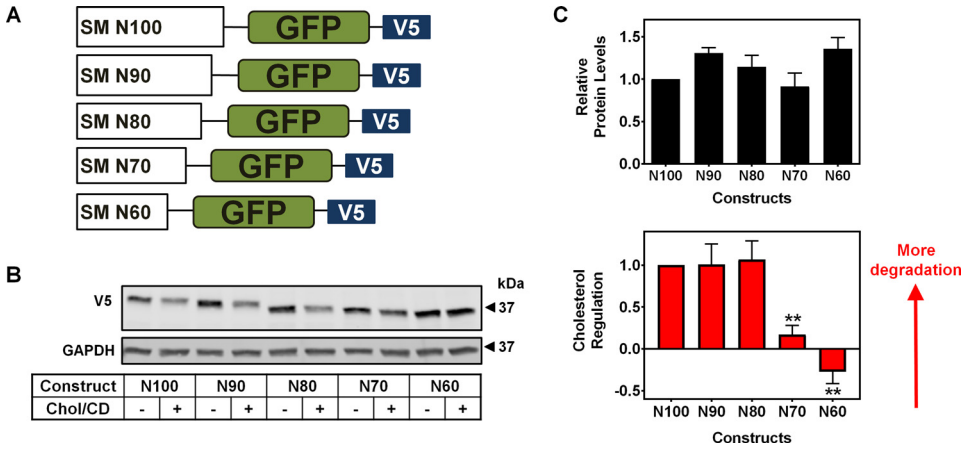

Figure 2. Truncations of SM N100 reveal a 20-residue region required for cholesterol regulation. *A,* schematic of truncation mutants of SM N100. All constructs contain GFP fused to the C-terminal end of SM N100 and contain a V5 epitope tag. *B,* CHO-7 cells were transfected for 24 h with the indicated SM N100 constructs (0.25 μg of expression plasmid and 0.75 μg of pTK-empty vector). Cells were then pre-treated overnight with compactin (5 μM) and mevalonate (50 μM). The next day, cells were treated for 8 h with or without Chol/CD (20 μg/ml). The Western blot is representative of at least three independent experiments. *C,* densitometric analyses of Western blot in *B*. Data are presented as mean + S.E. from at least three independent experiments. Significant changes in cholesterol regulation or protein levels compared with WT SM N100 are indicated: **, $p \leq 0.01$.

(Fig. 2, *B* and *C*). Cholesterol regulation of SM N80 reached the same level as WT SM N100 (Fig. 2, *B* and *C*), indicating that a region between residues 60 and 80 is necessary for cholesterol-mediated turnover of SM N100.

Alanine-scanning mutagenesis reveals a residue required for cholesterol regulation

To locate short linear motifs required for the cholesterol-regulated degron, we performed systematic site-directed mutagenesis of SM N100 by mutating every second amino acid to alanine and testing each mutant for cholesterol regulation (Fig. 3*A*). We expected point mutations that diminished cholesterol-mediated turnover would reveal important residues or motifs. Such approaches have been used to identify important residues in other cholesterol-related proteins such as Insig-2 (23), Scap (24), and Niemann-Pick C2 (25).

We quantified the protein expression (Fig. 3*B*) and cholesterol regulation (Fig. 3*C*) of all 47 alanine mutants, normalized to WT SM N100. To increase stringency and reduce false discovery rates, we further imposed an arbitrary threshold, with relative protein expression levels below 0.5 or above 1.5 and relative cholesterol regulation below 0.8 or above 1.2 required to accept any observed statistical significance. We noted V32A did not express, whereas W2A and L70A expressed very poorly (Fig. 3*B*). Val-32 is located within the known re-entrant loop (8), so the mutation could be a destabilizing mutation that affects the native structure of the re-entrant loop.

One mutant, L42A, containing a mutated residue at the boundary of the exiting re-entrant loop (Fig. 1*A*), showed significantly higher protein levels and blunted cholesterol regulation (Fig. 3, *B* and *C*). However, alanine mutations of the neighboring residues (V41A and S43A) had normal cholesterol regulation (data not shown). Taken together, our alanine-scanning approach failed to identify short linear motifs required for the cholesterol-mediated turnover of SM N100, indicating that other approaches are needed to elucidate the degron.

SM N100 varies in protein expression and cholesterol regulation between species

Next, we took a comparative biology approach to identify motifs necessary for cholesterol regulation. SM N100 is well-conserved in mammals, but this region is lacking in lower eukaryotes such as yeast (2). We have also demonstrated that hamster full-length SM undergoes cholesterol-mediated turnover, highlighting the mammalian conservation of SM regulation (2). We hypothesized that SM N100 cholesterol regulation differs in lower order vertebrates due to evolutionary divergence giving rise to different primary amino acid sequences.

We aligned the first 100 amino acids of human, chicken, zebrafish, and lamprey SM (Fig. 4*A*). These animals were chosen to represent different evolutionary time points, with the lamprey, a jawless fish, being one of the earliest known vertebrates. Our multiple sequence alignment showed 14 identical residues, which were mostly in the first half of SM N100 (Fig. 4*A*). Cholesterol regulation might be expected to emerge with species like chicken, which are more closely conserved with human SM N100 (62% similarity), whereas the most divergent sequences such as lamprey (43% similarity) (Fig. 4*B*) may not be cholesterol-regulated. To test this, we cloned SM N100-GFP constructs for each of these species and tested their protein expression and cholesterol regulation. Protein expression of chicken SM N100 was significantly higher than human SM N100, whereas both zebrafish and lamprey had low expression (Fig. 4, *C* and *D*). Unexpectedly, chicken SM N100, which had the highest similarity and identity to human SM N100 (Fig. 4*B*), showed blunted cholesterol regulation (Fig. 4, *C* and *D*). In contrast, zebrafish SM N100 remained cholesterol-regulated, and lamprey SM N100 was stabilized by cholesterol (Fig. 4, *C* and *D*). Therefore, these divergent sequences appear to affect both protein expression and cholesterol regulation in an unpredictable manner.

We then investigated the overall protein sequence variability. We observed high sequence variability between residues 41–70 and 91–100 (Fig. 4*E*), consistent with the lack of conservation

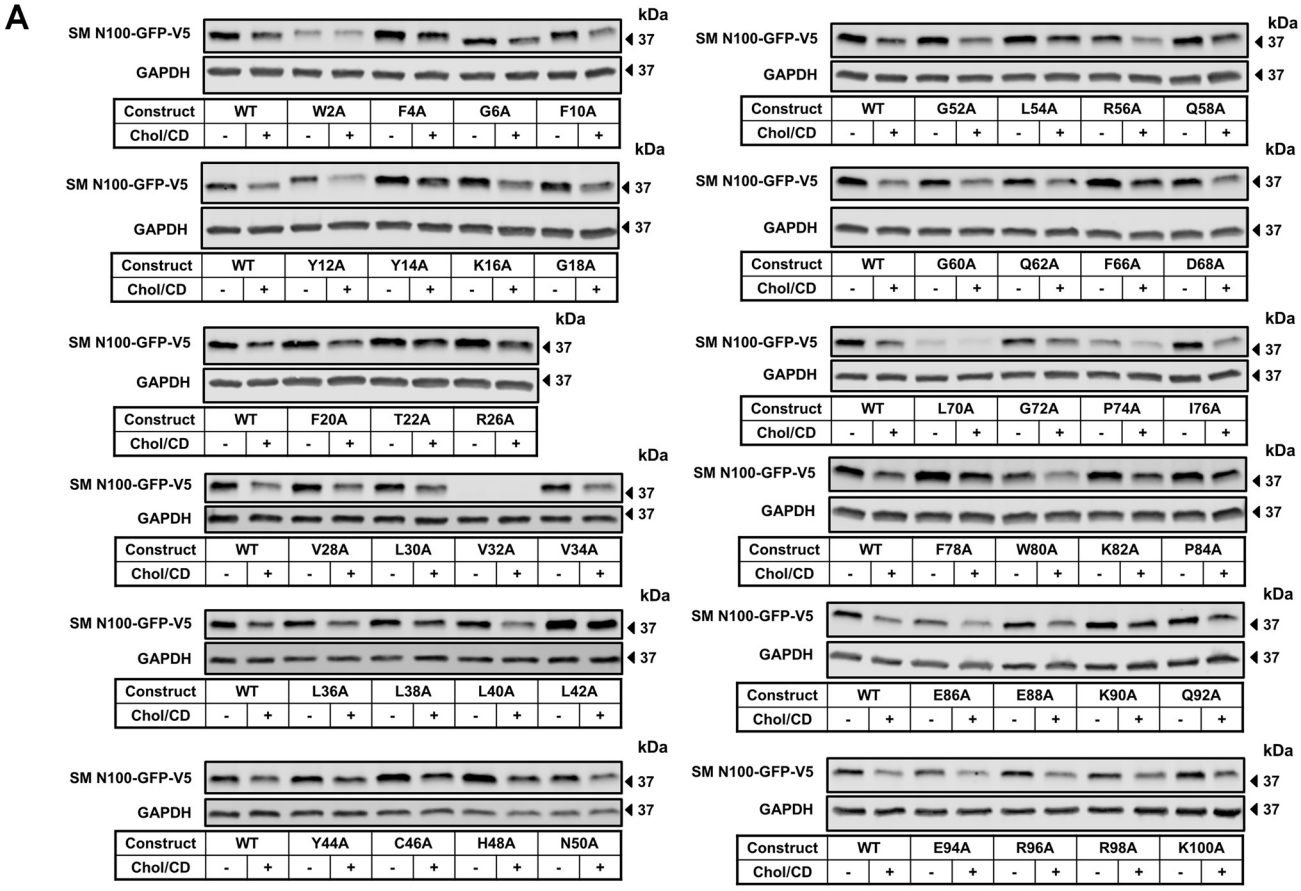
A
SM N100-GFP-V5
GAPDH
kDa
37
Construct
Chol/CD
WT
W2A
F4A
G6A
F10A
Y12A
Y14A
K16A
G18A
F20A
T22A
R26A
V28A
L30A
V32A
V34A
L36A
L38A
L40A
L42A
Y44A
C46A
H48A
N50A
G52A
L54A
R56A
Q58A
G60A
Q62A
F66A
D68A
L70A
G72A
P74A
I76A
F78A
W80A
K82A
P84A
E86A
E88A
K90A
Q92A
E94A
R96A
R98A
K100A

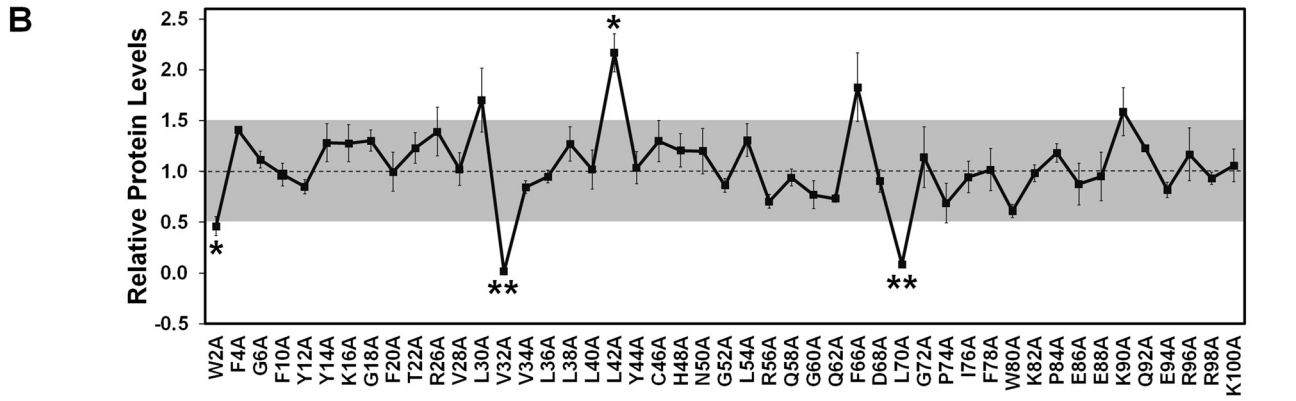
B
Relative Protein Levels
2.5
2.0
1.5
1.0
0.5
0.0
-0.5
*
**
W2A F4A G6A F10A Y12A Y14A K16A G18A F20A T22A R26A V28A L30A V32A V34A L36A L38A L40A L42A Y44A C46A H48A N50A G52A L54A R56A Q58A G60A Q62A F66A D68A L70A G72A P74A I76A F78A W80A K82A P84A E86A E88A K90A Q92A E94A R96A R98A K100A

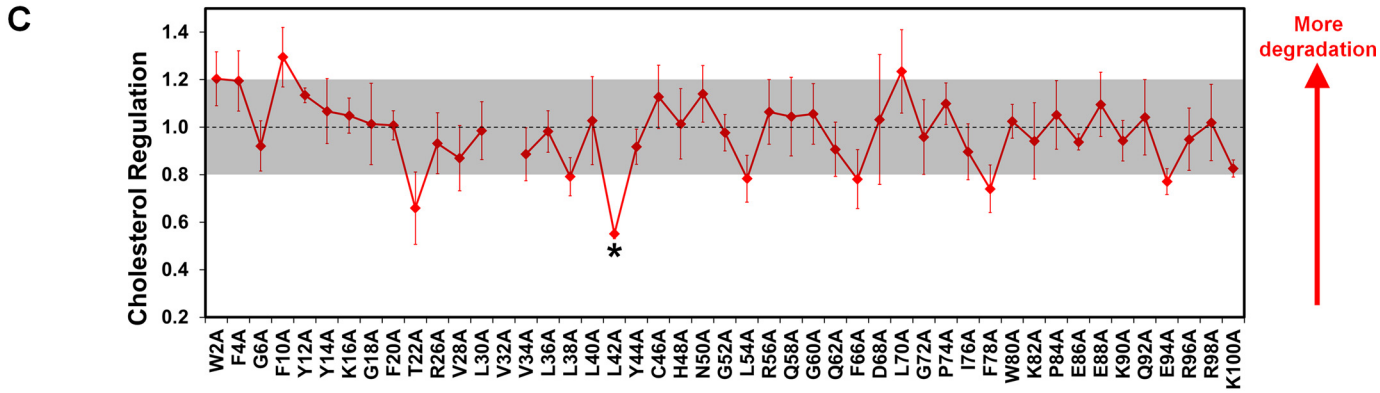
C
Cholesterol Regulation
1.4
1.2
1.0
0.8
0.6
0.4
0.2
*
More degradation
W2A F4A G6A F10A Y12A Y14A K16A G18A F20A T22A R26A V28A L30A V32A V34A L36A L38A L40A L42A Y44A C46A H48A N50A G52A L54A R56A Q58A G60A Q62A F66A D68A L70A G72A P74A I76A F78A W80A K82A P84A E86A E88A K90A Q92A E94A R96A R98A K100A

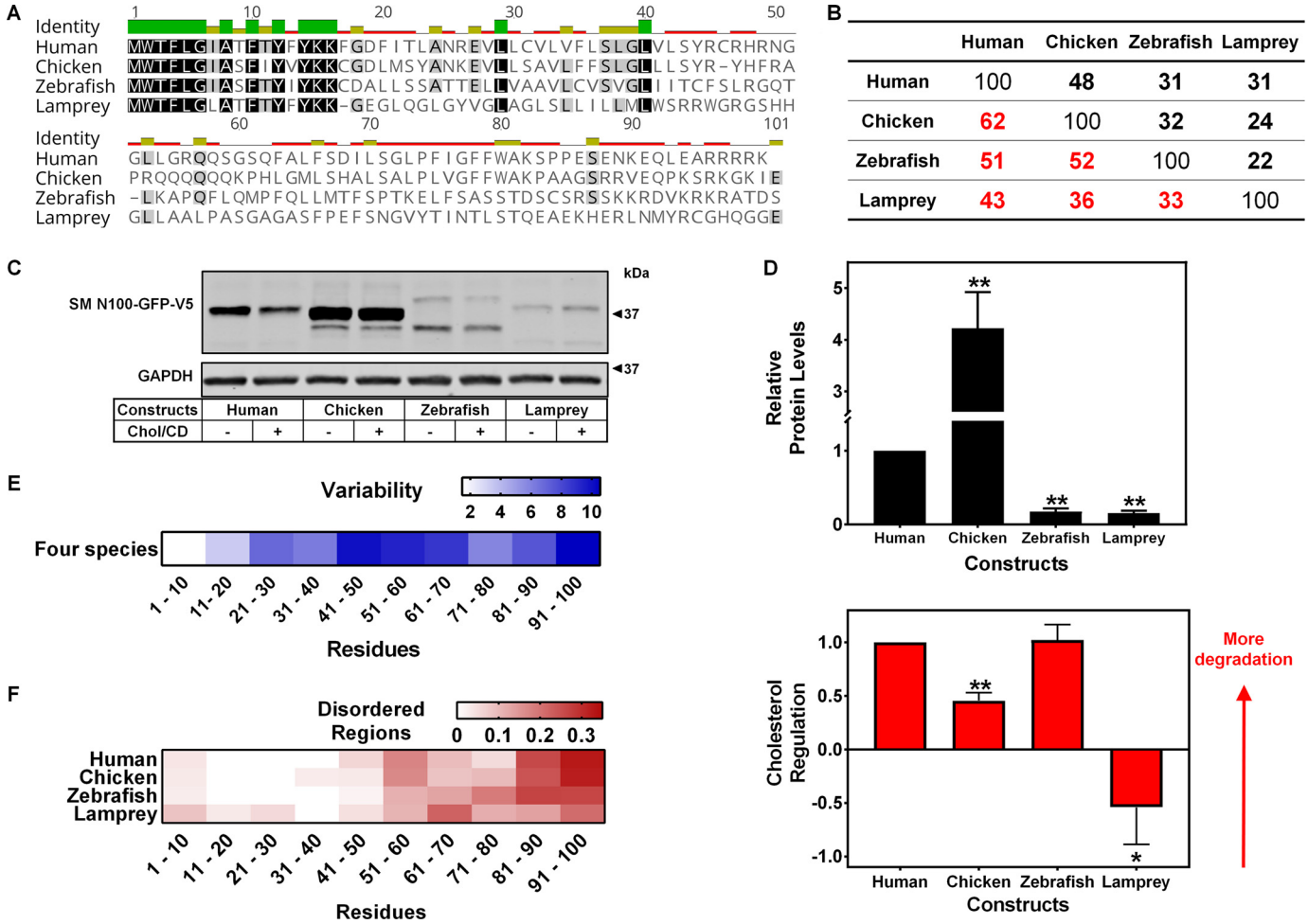

	Human	Chicken	Zebrafish	Lamprey
Human	100	48	31	31
Chicken	62	100	32	24
Zebrafish	51	52	100	22
Lamprey	43	36	33	100

Figure 4. Evolutionary variants of SM N100 display distinct protein expression levels. *A,* first 100 amino acids of human, chicken, zebrafish, and lamprey SM were aligned with Geneious 9.1.5 using default settings. *Green bars* indicate pairwise identity of 100%. *Yellow bars* indicate pairwise identity of 30–100%. *Red bars* indicate pairwise identity below 30%. *B,* pairwise comparisons of sequence identity and similarity in *A* were determined using Geneious 9.1.5. *Boldface red numbers* indicate percentage similarity and *boldface black numbers* refer to percentage identity. *C,* CHO-7 cells were transfected for 24 h with the indicated SM N100 species constructs (0.25 μg of expression plasmid and 0.75 μg of pTK-empty vector). Cells were then pre-treated overnight with compactin (5 μM) and mevalonate (50 μM). The next day, cells were treated for 8 h with or without Chol/CD (20 μg/ml). The Western blot is representative of at least three independent experiments. *D,* densitometric analyses of Western blot in *C*. Data are presented as mean + S.E. from at least three independent experiments. Significant changes in cholesterol regulation or protein levels compared with human SM N100 are indicated: *, $p \leq 0.05$, or **, $p \leq 0.01$. *E,* heat map showing the SM N100 protein sequence variability using the Wu-Kabat variability coefficient. *F,* heat map shows frequency of disordered regions in 10-residue windows for each SM N100 species variant.

from the sequence alignment (Fig. 4*A*). The high variability and low conservation prompted us to determine whether disordered regions were present in SM N100, as disordered regions tend to be evolutionarily less conserved, exhibiting higher variability (26). More importantly, disordered regions are recognized as essential features in degrons (18, 20–22). Next, we obtained disordered predictions from 13 predictors. In both human and chicken SM N100, residues 91–100 were most frequently predicted to be disordered, followed by residues 81–90 and 51–60 (Fig. 4*F*). As expected, the disordered distribution was different in the two more distant species, zebrafish and lamprey. Taken together, we propose that the different cholesterol regulation and protein expression is not due to primary sequence divergence alone. Instead, structural differences, such as disordered regions, may explain the different responses observed in each degron variant.

Conserved yeast degron residues are important for SM N100 cholesterol regulation

We next considered known degron examples in the literature. One of the earliest-identified and most well-studied degrons is Deg1, which contains an amphipathic helix necessary for degradation (12), and it is degraded by Doa10, the yeast homolog of MARCH6 (14). We compared Deg1 with our SM

Figure 3. Leu-42 in SM N100 is required for normal cholesterol regulation. *A,* CHO-7 cells were transfected for 24 h with the indicated SM N100 constructs (0.25 μg of expression plasmid and 0.75 μg of pTK-empty vector). Cells were then pre-treated overnight with compactin (5 μM) and mevalonate (50 μM). The next day, cells were treated for 8 h with or without Chol/CD (20 μg/ml). The Western blots are representative of at least three independent experiments, and the data are presented as mean ± S.E. *B* and *C,* densitometric analyses of Western blots in *A*. The *gray-shaded regions* represent an arbitrary range to choose a statistical significance threshold. The relative protein levels and cholesterol regulation were normalized to WT SM N100, which was set at 1 as shown by the *black dashed lines*. Significant changes in cholesterol regulation or protein levels compared with WT SM N100 are indicated: *, $p \leq 0.05$, or **, $p \leq 0.01$.

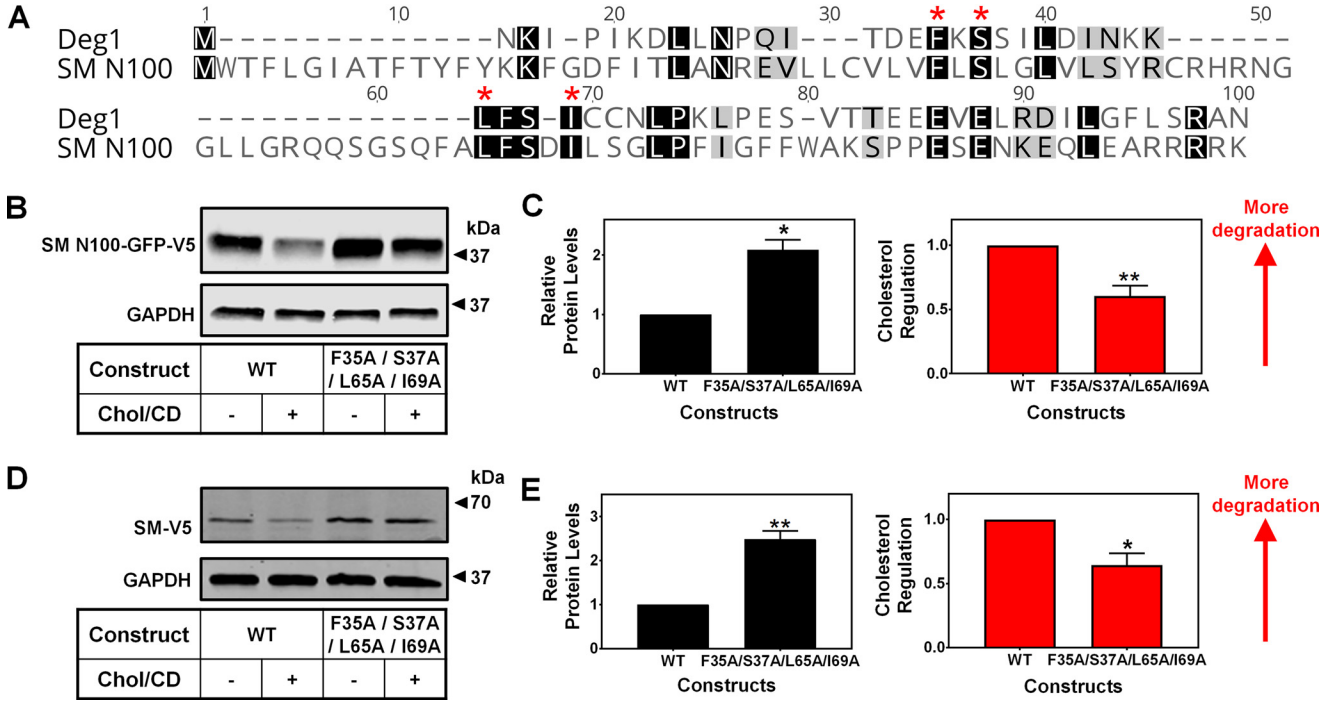

Figure 5. Four conserved degron residues of Deg1 are required for SM cholesterol-mediated turnover. *A*, conservation of the Deg1 degron with SM N100. Deg1 degron sequence belonging to the Matα2 protein was aligned with SM N100 in Geneious 9.1.5 with default settings. *Red asterisks* indicate the critical residues of Deg1, which matched SM N100. *B* and *D*, CHO-7 cells were transfected for 24 h with the indicated SM N100 constructs (0.25 μg of expression plasmid and 0.75 μg of pTK-empty vector) or SM full-length constructs (1 μg of expression plasmid). Cells were then pre-treated overnight with compactin (5 μM) and mevalonate (50 μM). The next day, cells were treated for 8 h with or without Chol/CD (20 μg/ml). The Western blot is representative of at least three independent experiments. *C* and *E*, densitometric analyses of Western blots in *B* and *D*, respectively. Data are presented as mean + S.E. from at least three independent experiments. Significant changes in cholesterol regulation or protein levels compared with WT are indicated: *, $p \leq 0.05$; **, $p \leq 0.01$.

N100 degron through a pairwise alignment, and we observed SM N100 has 27% identity and 42% similarity with the 62 residues of Deg1. Moreover, we observed that four critical amphipathic helix residues of Deg1 (12) aligned with SM N100. These residues corresponded to Phe-35, Ser-37, Leu-65, and Ile-69 in SM N100 (Fig. 5*A*). Using site-directed mutagenesis, we produced a quadruple alanine mutant F35A/S37A/L65A/I69A in both SM N100 and full-length SM. In both cases, protein levels increased for the mutants, whereas the cholesterol regulation was blunted (Fig. 5, *B–E*). This suggests that these four conserved degron residues play an important role in SM cholesterol-mediated turnover.

A helical structure is present within the second half of SM N100

Amphipathic helices have been implicated as degrons of other proteins (12, 16–19). We hypothesized that there may be an amphipathic helix in the second half of SM N100, which is required for SM cholesterol-mediated turnover. We first determined any secondary structural elements in full-length SM with PSIPRED version 3.3 and focused on residues 50–100. We identified secondary helix structures from residues 62 to 73 and 90 to 99 (Fig. 6*A*). We also used PEP-FOLD3 and identified a helical structure between residues 61 and 71 (Fig. 6*B*), but no other secondary structure existed for the rest of the second half of SM N100 (data not shown).

To verify this, we performed molecular dynamics simulations of SM N100 in an all-atomistic representation. Two independent molecular dynamics simulations with different *ab initio* modeled starting structures were performed (Fig. 6, *C* and *D*). The total computing time was 2.4 μs. Simulation 1 showed residues 59–61 and 68–71 formed a 3_{10}-helix (Fig. 6*C*), whereas simulation 2 showed residues 63–75 formed the longest and most stable α-helix (Fig. 6*D*). The data from the molecular dynamics simulations and secondary structure prediction servers support the presence of a helical structure within the second half of SM N100.

Amphipathic helix of SM N100 is necessary for cholesterol regulation

Previously, we ruled out the existence of any hydrophobic transmembrane regions in the second half of SM N100 (8). Here, we considered the possibility of an amphipathic helix that is weakly associated with the ER membrane instead of a hydrophobic transmembrane domain. A helical wheel representation of SM N100 residues 62–73 revealed the hydrophobic moment, a measure of helix amphipathic character, for SM N100 (μ_H = 0.54) (Fig. 7*A*) was comparable with that of Deg1 (μ_H = 0.51) (Fig. 7*D*). We next removed the SM N100 amphipathic helix (Δ62–73) and found that this deletion abolished cholesterol regulation (Fig. 7, *B* and *C*), suggesting a crucial role of this amphipathic helix in cholesterol regulation of SM. We then showed that Deg1 fused to GFP is not cholesterol-regulated (Fig. 7, *E* and *F*), demonstrating that cholesterol regulation of a protein is not reliant on an amphipathic helix alone. Furthermore, Deg1-GFP levels were significantly lower than SM N100, consistent with Deg1 being intrinsically unstable as would be

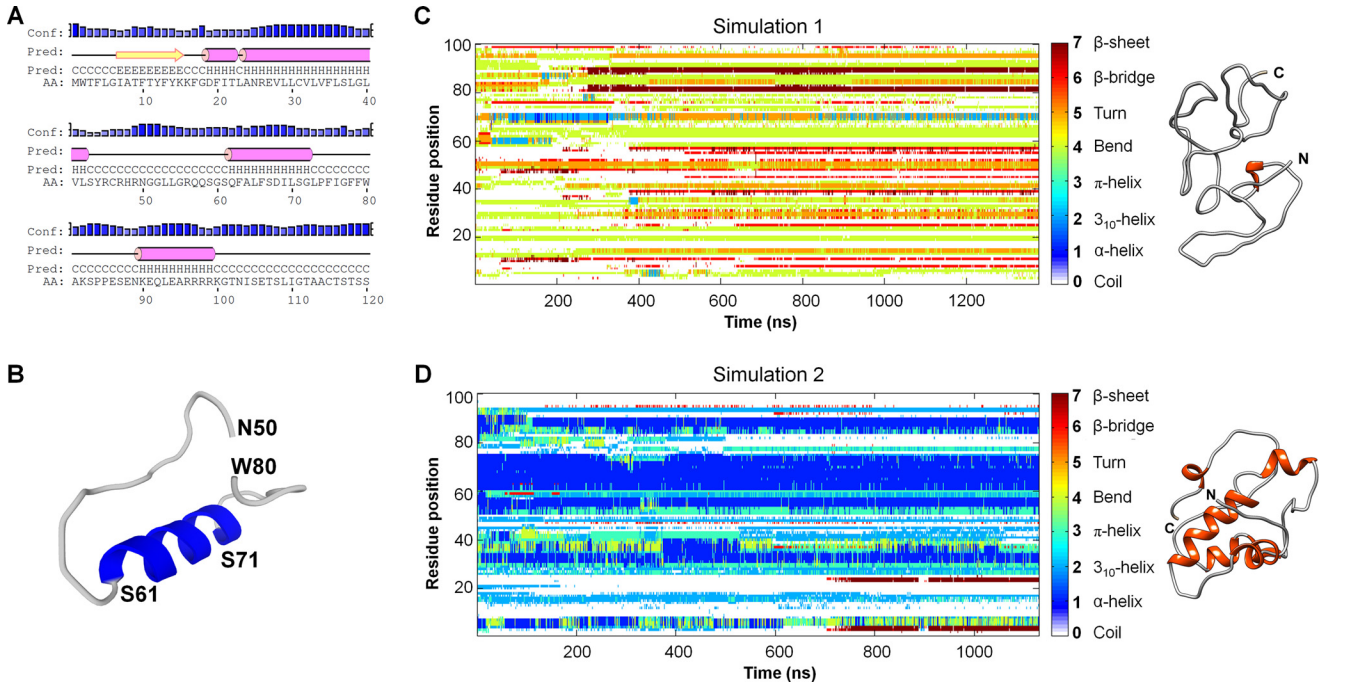

Figure 6. Second half of SM N100 contains a helix. *A,* secondary structure prediction of full-length SM by PSIPRED version 3.3 with results from only the first 120 amino acids shown. The prediction (*pred*) row shows helices as *pink rods* and strands as *yellow arrows*. Amino acid residue (*AA*) positions are shown *below* each amino acid. The confidence level (*conf*) is shown on the top. *Higher bars* with *darker shades* of *blue* represent higher prediction confidence. *B,* residues 50–80 of SM N100 were analyzed in PEP-FOLD3. Secondary predictions with helical structures are highlighted in *blue*. *C* and *D,* two independent molecular dynamics simulations were performed with different *ab initio* modeled starting structures (see "Experimental procedures"). Secondary structure assignment of SM N100 for simulation 1 (*C*) and simulation 2 (*D*), respectively, is plotted as a function of time. The secondary structure is color-coded (*white,* coil; *dark blue,* α-helix; *light blue,* 3_{10} helix; *turquoise,* π-helix; *green,* bend; *orange,* turn; *red,* β-bridge; *dark red,* β-sheet). The representative structures shown on the *right* were extracted from the last time frame at 1.3 μs for simulation 1 and 1.1 μs for simulation 2.

expected for a degron responsible for the turnover of a short-lived protein, MATα2 (12). We proposed the amphipathic helix is membrane-associated, allowing the helix to sense membrane cholesterol. Amphipathic helices have been reported to be involved in sensing membrane lipids or introducing membrane curvature, both of which are important in mediating protein–lipid interactions (27). Thus, it is likely that a cytosolically exposed helix cannot substitute the SM N100 amphipathic helix. We replaced the amphipathic helix with an α-helix (EAEIKPLAQSHAT) of myoglobin (Protein Data Bank code 3RGK) (28), one of the earliest and best studied globular cytosolic proteins with a high percentage of helices (29). As expected, SM N100 showed blunted cholesterol regulation when the highly charged α-helix (Fig. 7*G*) substituted the SM N100 amphipathic helix (Fig. 7, *H* and *I*). Hence, we have identified a critical amphipathic helix required for the cholesterol-regulated turnover of SM N100.

Hydrophobicity is a key feature involved in cholesterol regulation of SM N100

As mentioned, SM N100 lacks any obvious membrane attachment point in the second half, and it is possible the amphipathic helix is only partially embedded in the membrane as exemplified by other known amphipathic helices (27). Increased cholesterol levels in the membrane can thicken the membrane (30) and perhaps induce dissociation of the partially associated amphipathic helix, leading to proteasomal degradation. If the attachment were stronger, increased cholesterol would be unlikely to eject this region from the membrane. We decided to test this by replacing the SM N100 amphipathic helix with a re-entrant loop that would retain the cytosolic orientation of the C-terminal end of SM N100. To this end, we replaced the amphipathic helix of SM N100 with re-entrant loops deduced from membrane topological studies of two ER membrane proteins, GOAT (YFSYLLFFPALLGGSL) and HHAT (WMLAYVFYYPVLHNG) (31–33). Both loops are very hydrophobic with minimal amphipathic character, as shown by their helical wheel representations (Fig. 8*A*).

We next tested the cholesterol regulation of these two new constructs. Surprisingly, SM N100 remained cholesterol-regulated when the two hydrophobic loops replaced the amphipathic helix, despite having very low expression (Fig. 8, *B* and *C*). Because these hydrophobic loops permit cholesterol regulation, perhaps the overall hydrophobicity is more important in determining cholesterol regulation than the amphipathic character. From the 11 human SM N100 constructs cloned in this study with variations in this region (Fig. 8*D*), we observed a linear relationship between cholesterol regulation and hydrophobicity of the amphipathic helix region (Fig. 8*E*). Single point alanine substitutions in the amphipathic helix retained cholesterol regulation (Fig. 3), possibly due to hydrophobicity being unchanged. In contrast, large reductions of hydrophobicity, such as introducing a hydrophilic myoglobin helix, blunt cholesterol regulation (Fig. 7, *G–I*). Overall, we calculated that at least two-thirds of the variation ($R^2 = 0.70$) (Fig. 8*E*) in cholesterol regulation are determined by hydrophobicity of the helical region between residues 62 and 73.

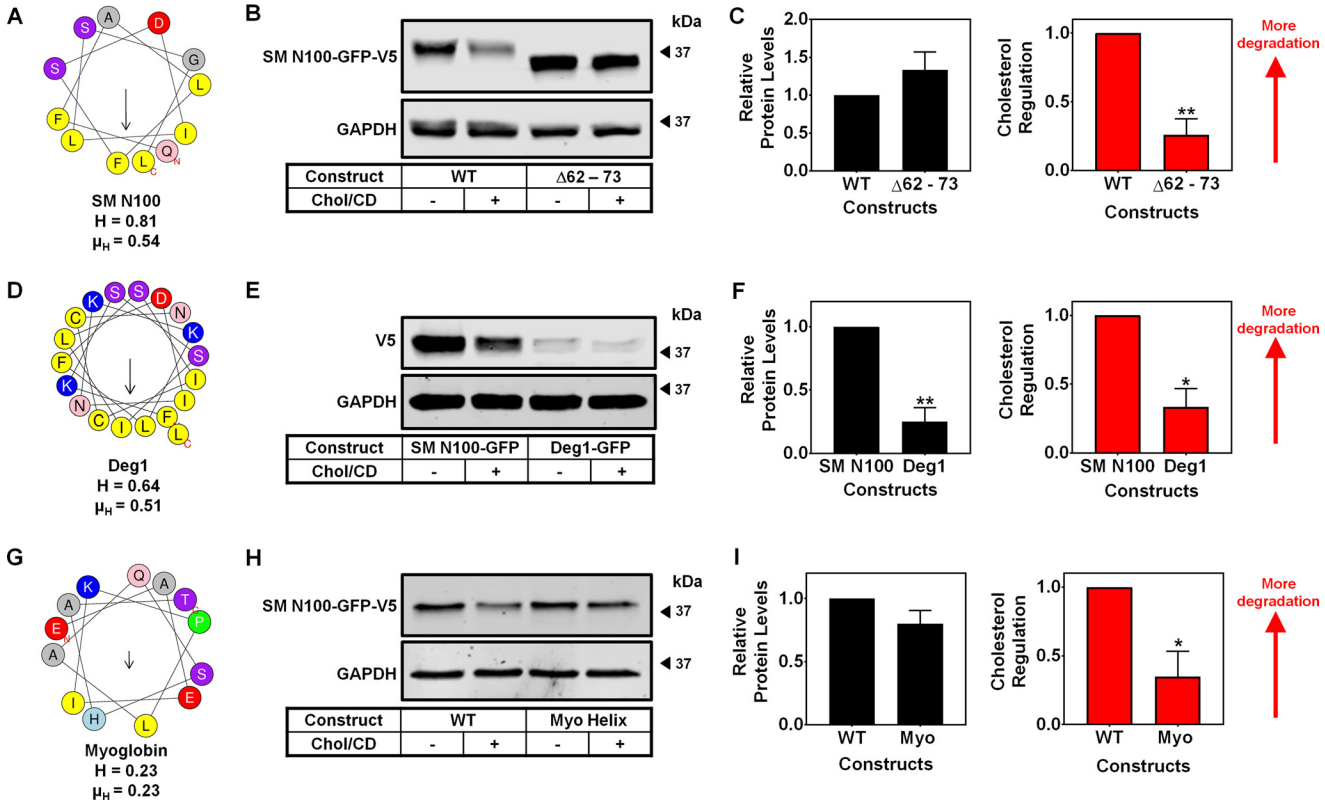

Figure 7. Amphipathic helix of SM N100 is necessary for cholesterol regulation. *A, D,* and *G,* helical wheel representations of amphipathic helices generated from HeliQuest. The *arrows* indicate the magnitude and direction of the hydrophobic moment. The hydrophobicity (*H*) and hydrophobic moment (μ_H) from HeliQuest are also shown. *B, E,* and *H,* CHO-7 cells were transfected for 24 h with the indicated constructs (0.25 μg of expression plasmid and 0.75 μg of pTK-empty vector). Cells were then pre-treated overnight with compactin (5 μM) and mevalonate (50 μM). The next day, cells were treated for 8 h with or without Chol/CD (20 μg/ml). The Western blots are representative of at least three independent experiments. *C, F,* and *I,* densitometric analyses of Western blots in *B, E,* and *H*. Data are presented as mean + S.E. from at least three independent experiments. Significant changes in cholesterol regulation or protein levels compared with WT SM N100 are indicated: *, $p \leq 0.05$; **, $p \leq 0.01$.

Amphipathic helix forms in a membrane-like matrix

We performed circular dichroism on a synthetic peptide made up of residues from the amphipathic helix of SM N100 (residues Gln-62–Leu-73). Addition of a non-ionic detergent, *n*-dodecyl β-D-maltoside as a membrane-like matrix, to the buffer promoted its transition from a disordered state to a helical structure, as indicated by the local minimum at 206 nm (Fig. 9*A*).

Therefore, the amphipathic helix is likely to form in contact with the ER membrane, as modeled here by the detergent micelles. We also analyzed a synthetic peptide from residues 50 to 60 of SM N100, the predicted disordered region (Fig. 4*F*). The peptide remained disordered with or without the addition of *n*-dodecyl β-D-maltoside (Fig. 9*B*).

Disordered region of SM N100 promotes basal turnover

Degrons are often characterized by disordered regions as these stretches are necessary for feeding into the proteasome (20–22). We hypothesized that the amphipathic helix undergoes a transition to a disordered region when cholesterol ejects it from the membrane. This gives a 12-residue hydrophobic stretch, and together with the disordered stretch before the helix (residues 50–60) (Fig. 4*F*), there should be sufficient length for engagement with the proteasome for degradation (21).

To test this, we replaced the amphipathic helix with a disordered flexible linker sequence containing glycine, alanine, and serine residues (34). Replacing the amphipathic helix with this disordered stretch blunted cholesterol regulation but did not affect basal protein turnover (Fig. 10, *A* and *B*). In contrast, deletion of the disordered region from residues 50 to 60 (Δ50–60) increased basal protein levels, but cholesterol regulation remained the same as WT (Fig. 10, *A* and *B*). Although the disordered replacement failed to promote degradation, it is possible that the difference in hydrophobicity of the disordered linker and a disordered amphipathic helix accounted for differences in degradation (Fig. 8*D*).

Cholesterol dissociates the second half of SM N100 from the membrane

We now have evidence that an amphipathic helix in the second half of SM N100 is necessary for cholesterol regulation (Fig. 7, *A–C*) and that it only forms within a membrane-like environment (Fig. 9*A*). To further examine the involvement of an amphipathic helix in the second half of SM N100, we determined the effects of *in vitro* cholesterol treatment of microsomes prepared from cells transfected with either WT SM N100 or SM N100 Δ48. SM N100 Δ48 lacks the re-entrant loop but contains the amphipathic helix. We predicted that this truncated protein would be less membrane-associated and that

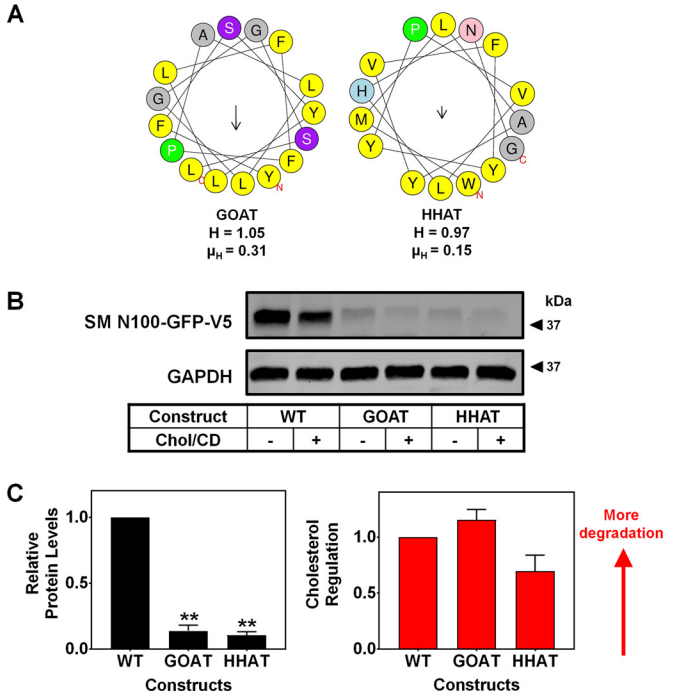

D

Human SM N100 Constructs	Hydrophobicity (H)	Cholesterol Regulation
WT	0.81	1.0
Q62A	0.85	0.91
F66A	0.69	0.78
D68A	0.90	1.03
L70A	0.69	1.24
G72A	0.84	0.96
F35A/S37A/L65A/I69A	0.57	0.60
Δ62-73	0.00	0.26
Myo helix	0.23	0.35
GOAT	1.05	1.15
HHAT	0.97	0.70
Linker	0.06	0.41
Non-human Constructs	**Hydrophobicity (H)**	**Cholesterol Regulation**
Chicken SM N100	0.79	0.46
Zebrafish SM N100	0.60	1.02
Lamprey SM N100	0.46	-0.54
Deg1	0.64	0.33

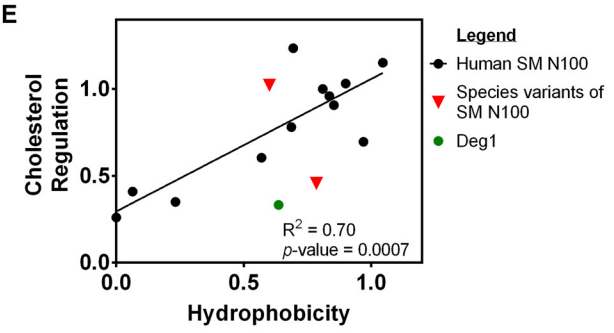

Figure 8. SM N100 cholesterol regulation is dependent on the hydrophobicity of residues 62–73. *A,* helical wheel representations of amphipathic helices generated from HeliQuest. The *arrows* indicate the magnitude and direction of the hydrophobic moment. The hydrophobicity (*H*) and hydrophobic moment (μ_H) from HeliQuest are also shown. *B,* CHO-7 cells were transfected for 24 h with the indicated constructs (0.25 μg of expression plasmid and 0.75 μg of pTK-empty vector). Cells were then pre-treated overnight with compactin (5 μM) and mevalonate (50 μM). The next day, cells were treated for 8 h with or without Chol/CD (20 μg/ml). The Western blot is representative of at least three independent experiments. *C,* densitometric analyses of Western blot in *B*. Data are presented as mean + S.E. from at least three independent experiments. Significant changes in cholesterol regulation or protein levels compared with SM N100 are indicated: **, $p \leq 0.01$. *D,* data showing the hydrophobicity of residues 62–73 in human SM N100, non-human SM N100, and Deg1. For replacement of the amphipathic helix mutations, hydrophobicity is obtained from the new sequence that replaced the amphipathic helix. Cholesterol regulation is obtained from densitometric analyses of each construct from the Western blots. *E,* linear regression line obtained using hydrophobicity and cholesterol regulation in *D*. Non-human SM N100 constructs were not used to generate the line of best fit. Lamprey SM N100 was not included in the plot as it gave a negative value for cholesterol regulation. Linear regression R^2 and *p* value were obtained from GraphPad Prism 7.02.

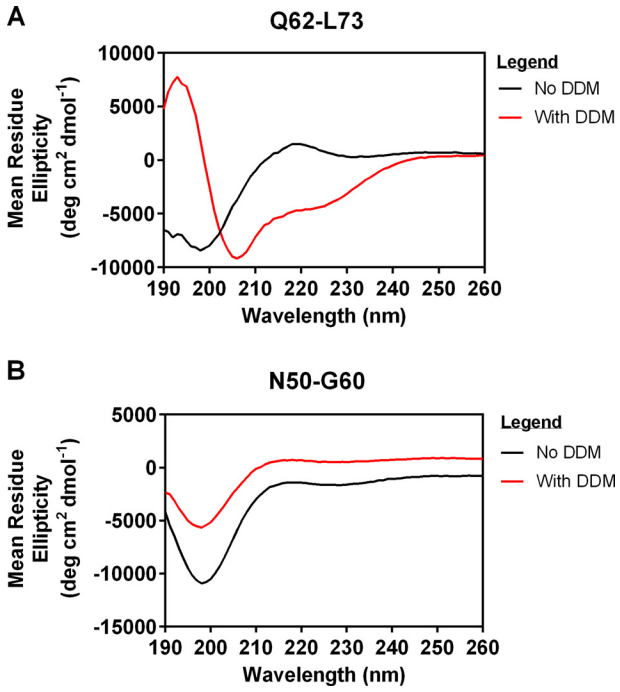

Figure 9. Evidence for amphipathic helix that forms with the presence of a membrane-like matrix. *A* and *B,* circular dichroism spectra of the amphipathic helix and disordered peptides at pH 7.0 in the presence (*red line*) or absence (*black line*) of *n*-dodecyl β-D-maltoside (*DDM*). Units are expressed as mean residue ellipticity.

cholesterol treatment would reduce this membrane association further.

On fractionation of the cell lysate to membrane pellet and supernatant, WT SM N100 was found almost exclusively in the pellet in agreement with our previous observations (8), whereas soluble GFP was found mostly in the supernatant as expected (Fig. 11*A*). Consistent with earlier experiments (Fig. 1, *C* and *D*), SM N100 Δ48 had lower protein expression (Fig. 11*A*). We accounted for the higher protein expression of WT SM N100, by loading a quarter of these samples to match the protein levels of SM N100 Δ48 (Fig. 11*B*). This allowed more direct comparison of pellet and supernatant fraction levels of the two proteins. We normalized the supernatant fraction to the pellet for each construct (Fig. 11*C*) and found that SM N100 Δ48 was more enriched (~6-fold) in the supernatant than WT SM N100. *In vitro* cholesterol treatment of the microsomes increased the proportion of SM N100 Δ48 levels in the supernatant, whereas WT SM N100 did not change significantly (Fig. 11*C*). These data demonstrated that the second half of SM N100 is more loosely associated with the membrane than WT SM N100 and is more readily dissociated in the presence of cholesterol.

Discussion

As a key control point in cholesterol biosynthesis, SM must be tightly regulated to control the rate of cholesterol biosynthe-

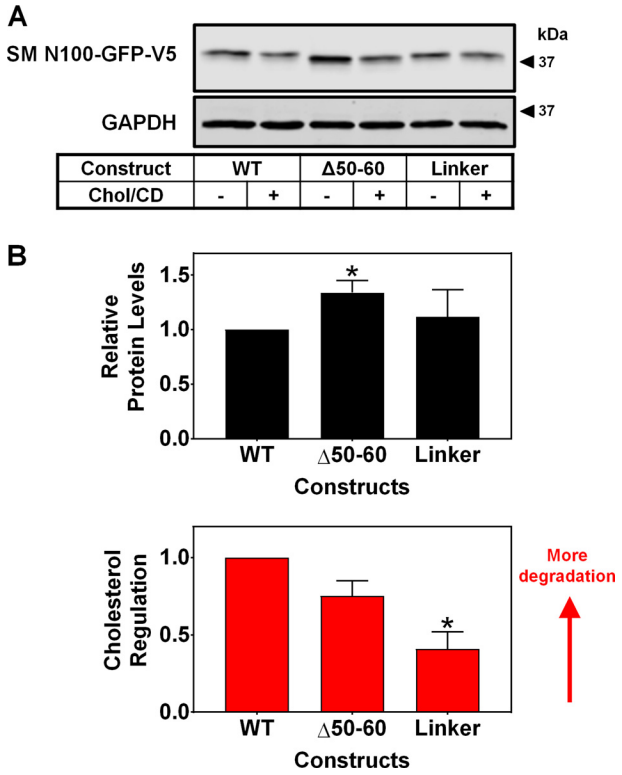

Figure 10. Disordered region from residues 50 to 60 is required for basal turnover of SM N100. *A,* CHO-7 cells were transfected for 24 h with the indicated constructs (0.25 μg of expression plasmid and 0.75 μg of pTK-empty vector). Cells were then pre-treated overnight with compactin (5 μM) and mevalonate (50 μM). The next day, cells were treated for 8 h with or without Chol/CD (20 μg/ml). The Western blot is representative of at least three independent experiments. *B,* densitometric analyses of Western blot in *A*. Data are presented as mean + S.E. from at least three independent experiments. Significant changes in cholesterol regulation or protein levels compared with WT SM N100 are indicated: *, $p \leq 0.05$.

sis in cells. At a post-translational level, our previous work demonstrated that cholesterol induces the degradation of SM via the ubiquitin–proteasome system, which requires the first 100 amino acids as the cholesterol-regulated degron (2). Therefore, two requirements of this homeostatic system are as follows: (i) adequate enzyme expression in low cholesterol conditions to enable sufficient cholesterol synthesis, and (ii) cholesterol responsiveness so that the enzyme is degraded in high cholesterol conditions.

In this study, we have examined these two parameters in more than 60 variants of SM N100, and we identified a key degron element required for its cholesterol-responsive degradation. We mapped this element through progressive deletions and assorted mutations to a critical region between residues 62 and 73. Molecular dynamics (Fig. 6, *C* and *D*) and circular dichroism studies (Fig. 9*A*) confirmed secondary structural predictions that this is an amphipathic helix, which is stabilized by a hydrophobic matrix representing ER membrane. Removing this region severely blunted cholesterol regulation, as did replacing it with a hydrophilic α-helix (Fig. 7). However, replacing this region with highly hydrophobic loops maintained cholesterol regulation but compromised protein expression (Fig. 8, *A–C*). Our initial intention with the GOAT and HHAT constructs was to swap the amphipathic helix with a re-entrant loop that irreversibly anchors the second half of SM N100 to the ER membrane, but it appears that we may have simply introduced very hydrophobic domains lacking in amphipathic character. Indeed, we found that the hydrophobicity of this domain was a key determinant of cholesterol regulation, accounting for 70% of the variability in response to 12 constructs tested with alterations in this domain (Fig. 8*E*). However, protein expression did not correlate with hydrophobicity of this domain. This is likely affected by changes along the length of SM N100, with certain single point mutations (Fig. 3*B*) compromising protein expression as much as large deletions (Fig. 1*D*).

Amphipathic helices are becoming a common feature of degrons (12, 16–19) and, as exemplified by one of the first degrons characterized, Deg1, part of the yeast transcription factor Matα2 (12). From our comparison of SM N100 with Deg1 (Fig. 5*A*), we identified four key residues required for normal cholesterol regulation of SM (Fig. 5, *B–E*). The four most important residues of Deg1 (12), all within the helical domain, aligned with two residues of SM N100 (Phe-35 and Ser-37) in the re-entrant loop (8) and two within the newly identified amphipathic helix (Leu-65 and Ile-69). The structure of SM is currently unknown, but the membrane-buried Phe-35 and Ser-37 are likely to be part of secondary structures, namely a hydrophobic helix within the ER. We previously showed that a cholesterol-responsive conformational change can be detected at the boundaries of the re-entrant loop, with flanking residues becoming less exposed with addition of cholesterol (8), perhaps due to membrane thickening (30).

As in its native yeast environment (12), Deg1 is highly unstable in a mammalian system, and unsurprisingly it is not cholesterol-responsive (Fig. 7, *E* and *F*). The SM N100 degron may be an example of evolutionary co-option, with natural selection repurposing an existing yeast degron, Deg1. Further refinement may then have followed to ensure that SM adequately expresses in low cholesterol conditions but is degraded in the presence of high cholesterol, thus providing mammals with another post-translational control point in cholesterol synthesis, beyond HMG-CoA reductase. How this evolutionary co-option may have occurred is obscure, especially considering that SM N100 in lamprey, a more primitive organism, has less similarity to Deg1 (13%) than the more recently evolved human SM N100 (42%).

An emerging theme in protein–membrane interactions is the ability of amphipathic helices to sense membrane lipid composition (27). For example, the transducer of ER stress, Ire1, uses an amphipathic helix to sense membrane irregularities (35). The important phosphatidylcholine-synthesizing enzyme, CTP:phosphocholine cytidylyltransferase, also has an amphipathic helix that detects packing defects in the ER membrane at low levels of phosphatidylcholine, and then when phosphatidylcholine levels are sufficient, it is pushed out of the membrane, losing its secondary structure (36). Could an analogous situation occur with SM? By thickening (30) or even flattening the membrane (37), could cholesterol help eject the amphipathic helix of SM N100, enabling its degradation? In support of this contention, we have shown that the amphipathic helix preferably forms in the presence of membranes, as mimicked by a detergent in our circular dichroism

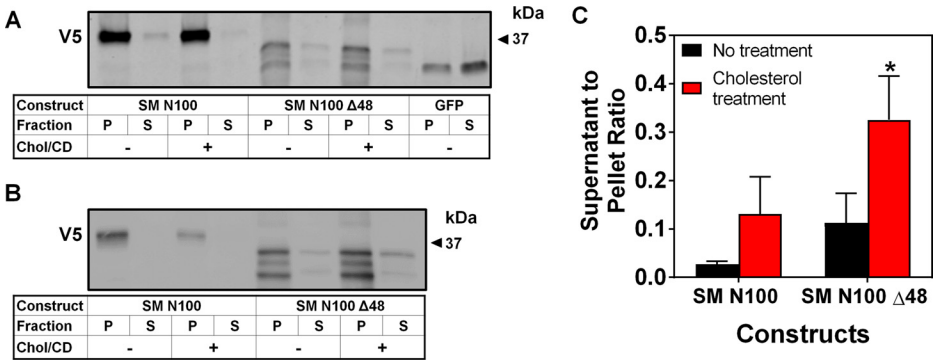

Figure 11. Second half of SM N100 associates weakly with the ER membrane and can dissociate upon cholesterol addition. *A,* CHO-7 cells were transfected for 24 h with the indicated constructs (4.2 μg of expression plasmid and 12.7 μg of pTK-empty vector). Cells were then pre-treated overnight with compactin (5 μM) and mevalonate (50 μM). The next day, microsomal membranes were isolated and treated with or without Chol/CD (20 μg/ml) for 30 min at 37 °C. The Western blot is representative of at least three independent experiments. Pellet is represented by (*P*) and supernatant is represented by (*S*). *B,* experiment was carried out as in *A* except protein expression was matched by loading a quarter of SM N100. The Western blot is representative of at least three independent experiments. *C,* densitometric analyses of Western blots in *A* and *B*. Data are presented as mean + S.E. from at least three independent experiments. Significant changes in supernatant to pellet ratios are as indicated: *, $p \leq 0.05$.

studies (Fig. 9*A*). Moreover, we found that the second half of SM N100 that contains the amphipathic helix, its only obvious means of membrane anchorage, is more loosely associated with the membrane and that this association is further loosened when cholesterol is added (Fig. 11).

Besides having an amphipathic helix, another common feature of a degron is a disordered region. Degrons can contain an intrinsically disordered region of 20–30 amino acids that can feed into the 26S proteasome (21), but the disordered stretch between residues 50 and 60 of SM N100 is too short. We propose that the neighboring amphipathic helix in SM N100 unravels after cholesterol-induced ejection from the membrane (analogous to CTP:phosphocholine cytidylyltransferase in response to sufficient phosphatidylcholine) to give the disordered length needed for the initiation of degradation (Fig. 12). Exposure of the unraveled helix, a hydrophobic region, may also promote degradation, given that exposed hydrophobic patches occur in many degrons (11, 38–40). Furthermore, degradation of proteins with amphipathic helical degrons have been shown to be dependent on their hydrophobicity (12, 17, 19). This is likely the case for SM N100, because hydrophobicity of the amphipathic helix was a strong determinant of the cholesterol-responsiveness of SM N100 (Fig. 8*E*). Without association of the helix to the membrane, the exposure of a highly hydrophobic surface could register as a sign of misfolding, possibly leading to recognition by the degradation machinery, including MARCH6, the E3 ubiquitin ligase for SM N100 (9). In line with this, Doa10, the yeast homolog of MARCH6, is proposed to degrade substrates by recognizing hydrophobic patches on its substrates (11).

More work is needed to test this hypothetical model, and the cholesterol-unresponsive mutants identified in this study will be important to add more mechanistic detail. For example, we aim to determine whether these mutants still interact with MARCH6 and become ubiquitinated. To conclude, our studies on the regulatory domain of SM, a flux-controlling enzyme in cholesterol synthesis, have identified key features that define this as the shortest known cholesterol-responsive degron and provide new insights into its molecular mechanism of action. Furthermore, we have discovered a remarkable congruence between this degron and the archetypal yeast degron, Deg1.

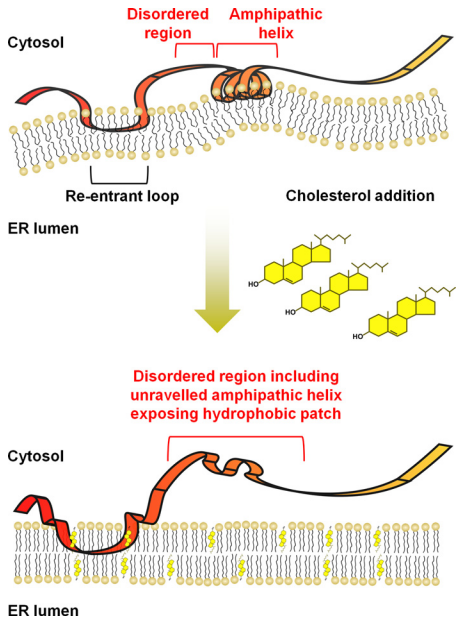

Figure 12. Working model on how the disordered region and amphipathic helix combine in the presence of excess cholesterol to mediate turnover of SM N100. SM N100 has a characteristic re-entrant loop and an amphipathic helix that is proposed to associate transiently with the ER membrane. In theory, the ER membrane may exhibit membrane curvature because of protein insertions and phospholipid asymmetry (*upper part of diagram*). Cholesterol can thicken and condense the ER membrane, flattening the membrane, resulting in the amphipathic helix being displaced from the ER membrane (*lower part of diagram*). The unraveling of the amphipathic helix upon displacement exposes the hydrophobic patch that constitutes the amphipathic helix. This extends the disordered region length, resulting in a sufficient number of disordered residues to facilitate the cholesterol-mediated turnover of SM N100.

Experimental procedures

Cell culture

CHO-7 cell lines (gifts of Drs. Goldstein and Brown, University of Texas Southwestern) were maintained in DMEM/F-12 media supplemented with 5% (v/v) newborn calf lipoprotein-deficient serum (LPDS), penicillin (100 units/ml), and streptomycin (100 μg/ml).

Plasmid constructs

The pTK-SM N100-GFP-V5 and pTK-SM-V5 constructs have been described previously (2). We used megaprimer site-directed mutagenesis (41) to mutate pTK-SM N100-GFP-V5 and pTK-SM-V5 to generate 49 alanine mutants as indicated in the figures. The pTK-SM N49-GFP-V5 construct was generated previously (8). All SM N100 truncation, domain replacement, and domain deletion constructs were generated from the pTK-SM N100-GFP-V5 plasmid using polymerase incomplete primer extension cloning (42). Nucleotide sequences coding for chicken SM N100 (NCBI accession no. NP_001181856.1), zebrafish SM N100 (NCBI accession no. NP_001103509.1), lamprey SM N100 (UniProt no. S4R6S3), and Deg1 (NCBI accession no. NP_009868.3) were codon-optimized for mammalian expression obtained in a pUC19 backbone (GenScript). These coding sequences were cloned into the human pTK-SM N100-GFP-V5 plasmid using the polymerase incomplete primer extension method (42), replacing the coding sequence of human SM N100. The identity of all cloned constructs were confirmed by Sanger sequencing. Primers for all cloned constructs in this study can be provided upon request.

Transfection

Prior to transfection, cells were refreshed with DMEM/F-12 media supplemented with 5% (v/v) LPDS without antibiotics. For cholesterol regulation assays, CHO-7 cells were seeded in 6-well plates at 2.5×10^5 cells per well and transfected the following day. Cells were transfected with 0.75 μg of pTK-empty vector DNA, 0.25 μg of expression plasmid DNA, and 4 μl of Lipofectamine-LTX for 24 h. For membrane *in vitro* cholesterol treatments, CHO-7 cells were seeded in 150-mm dishes and transfected with 12.7 μg of pTK-empty vector plasmid DNA, 4.2 μg of expression plasmid DNA, and 67.6 μl of Lipofectamine-LTX for 24 h.

Cholesterol regulation assays

Transfected CHO-7 cells were pre-treated in maintenance media containing compactin (5 μM) and mevalonate (50 μM) overnight to reduce basal cholesterol status. Cells were then treated with cholesterol complexed with methyl-β-cyclodextrin (CD) (20 μg/ml) for 8 h before harvesting cell lysates. The complexing process was performed as described previously (43).

Cell fractionation

Transfected CHO-7 cells were pre-treated in maintenance media containing compactin (5 μM) and mevalonate (50 μM) overnight to reduce basal cholesterol status. Microsomal membranes were harvested and prepared as described previously with modifications (8, 44). Briefly, cell lysates were centrifuged at 1,000 $\times$ *g* at 4 °C for 5 min, and the supernatant was subsequently centrifuged at 20,000 $\times$ *g* at 4 °C for 30 min to separate the cytosol and membrane fractions. Microsomal membrane pellets were resuspended in Buffer A (10 mM Hepes-KOH, pH 7.4, 10 mM KCl, 1.5 mM $MgCl_2$, 5 mM sodium EDTA, 5 mM sodium EGTA, and 250 mM sucrose). For *in vitro* cholesterol treatment, equal amounts of microsomal membrane proteins were treated with cholesterol complexed with CD (20 μg/ml) in Buffer A for 30 min at 37 °C. After treatment, microsomal membranes were centrifuged at 20,000 $\times$ *g* at 4 °C for 30 min to remove excess cholesterol. Equal proportions of pellet and supernatant were loaded for Western blotting.

Western blotting

Lysates from cells transiently expressing SM N100-GFP-V5 constructs were harvested as described previously (8). Lysates were equally loaded for SDS-PAGE separation and transferred onto nitrocellulose membranes. Membranes were blocked with 5% (w/v) skim milk/PBST and probed with mouse anti-V5 (1:5,000 dilution in 5% (w/v) skim milk/PBST; Life Technologies, Inc., catalog no. R960-25, lot no. 1831141) and rabbit anti-GAPDH (1:2,000 dilution in 5% (w/v) BSA/PBST; Cell Signaling Technology, catalog no. 2118, lot no. 10). After incubations with primary antibodies, blots were co-incubated with IRDye® 680RD donkey anti-rabbit IgG (1:10,000 dilution in 5% (w/v) skim milk/PBST; LI-COR, product no. 925-68073) and IRDye® 800CW donkey anti-mouse IgG (1:10,000 dilution in 5% (w/v) skim milk/PBST; LI-COR, product no. 926-32212). Membranes were then visualized using the Odyssey CLx (LI-COR). Western blots were quantified by densitometry using Image Studio Lite (version 5.2.5). Locations of molecular mass standards are indicated on the blots.

Molecular dynamics simulations

Because SM N100 does not share homology with any known experimentally resolved structure, we carried out two independent microsecond-time scale molecular dynamics simulations to extract detailed structural information. The starting structure of two molecular dynamics simulations was modeled using different methodologies. First, unbiased random dihedral assignment was performed to obtain a nearly linear chain of SM N100, and second, *ab initio* modeled structure using the on-line server QUARK (45). These two modeled structures enabled us to start two independent molecular dynamics simulations (simulation 1 for 1.3 μs and simulation 2 for 1.1 μs, respectively) for better sampling of folded conformations.

Molecular dynamics simulations were performed using the program GROMACS (46) by employing OPLS all-atom force field (47). The system was solvated using the TIP4P water representation (48). Periodic boundary conditions were used, and long-range electrostatic interactions were treated with the Particle Mesh Ewald summation (49). The real-space cutoff distance was set to 1.0 nm, and the van der Waals cutoff was set to 1.2 nm. A time step of 2 fs for numerical integration of the equations of motion was used. The protein was placed in a dodecahedral water box, large enough to contain the protein and at least 1.0 nm of solvent on all sides. The starting structures were subjected to energy minimization using the steepest descent method. Systems were simulated at 300 K and maintained by a V-rescale thermostat (50) with a time constant of 0.1 ps. Pressure coupling was done employing a Parrinello-Rahman (51) barostat using a 1-bar reference pressure and a time constant of 2 ps.

Bioinformatics predictions and sequence alignments

Sequence alignments were generated using Geneious 9.1.5 with default settings (52). Secondary structures were predicted using PSIPRED version 3.3 (53) and PEP-FOLD3 (54). Helical wheel diagrams were generated using HeliQuest (55). A total of 13 predictors for disordered regions were obtained from DisEMBL (56), DISOPRED3 (57), DisProt (58), GlobPlot2.3 (59), IUPred (60), PONDR (61–63), and PrDOS (64). For the sequence variability, values were obtained from the Protein Variability Server (65) using the Wu-Kabat variability coefficient (66).

Circular dichroism

The synthetic peptides were diluted to 60 μM for circular dichroism measurements. The Asn-50–Gly-60 peptide was initially dissolved in water and diluted with buffer (final concentration of 10 mM potassium phosphate, 50 mM sodium sulfate buffer, pH 7.0). The Gln-62–Leu-73 peptide was initially dissolved in 100% (v/v) DMSO and further diluted with buffer (final concentration of 10 mM potassium phosphate, 50 mM sodium sulfate buffer containing 0.01% (v/v) DMSO, pH 7.0). Circular dichroism spectra were recorded with a 0.5-mm path length cuvette and collected on the Chirascan circular dichroism spectrometer (Applied Photophysics) with constant nitrogen stream at ambient temperature of 25 °C. Each spectrum was recorded with a scan speed of 20 nm/min, bandwidth of 2 nm, and step of 1 nm. Spectrum presented is an average of three scans recorded from 190 to 260 nm with buffer subtracted from the peptide spectra in Pro-Data Viewer (Applied Photophysics).

Data presentation and statistical analysis

Relative protein levels for all SM N100, full-length SM, and Deg1 constructs were determined by normalizing to WT (human SM N100 or human full-length SM) as appropriate, which was set to 1. So for instance, a value of 2 would indicate the construct had double the protein level of WT. Cholesterol regulation was given as the proportion of protein degraded for each construct, normalized to the proportion of protein degraded for WT, which was set to 1. Values approaching zero on the cholesterol regulation scale indicate little or no cholesterol regulation, whereas a value of 1 would be the same as wild type. All Western blottings are representative of at least three independent experiments. Densitometry data from at least three independent experiments are presented as bar or line graphs. Densitometry data in bar graphs are presented as mean + S.E., whereas data in line graphs are presented as mean ± S.E. Statistical differences were determined by the Student's paired *t* test (two-tailed), where *p* values of $p \leq 0.05$ (*) and $p \leq 0.01$ (**) were considered statistically significant.

For the heat map of disordered region frequency distribution, the SM N100 protein for each species was divided into 10 parts, each containing 10-residue windows. The frequency distribution was determined by the cumulative number of predicted disordered residues within each 10-residue window from 13 predictors. The heat map for protein sequence variability was presented as the average of variability scores in each region as indicated in the figure.

Author contributions—N. K. C. and V. H. performed the experiments, analyzed, and interpreted the data. N. K. C. also generated the bulk of the bioinformatic analyses. N. J. and L. T. performed and provided data from molecular dynamics simulations. A. J. B. conceived the idea for the project and interpreted the data. All authors contributed to writing the paper, experimental designs, and approved the final version of the manuscript.

Acknowledgments—We thank the members of the Brown laboratory for critically reviewing this manuscript, and Isabelle Capell-Hattam, Hudson Coates, and Lydia Qian for contributions to preliminary experimental work.

References

1. Goldstein, J. L., and Brown, M. S. (2015) A century of cholesterol and coronaries: from plaques to genes to statins. *Cell* **161,** 161–172
2. Gill, S., Stevenson, J., Kristiana, I., and Brown, A. J. (2011) Cholesterol-dependent degradation of squalene monooxygenase, a control point in cholesterol synthesis beyond HMG-CoA reductase. *Cell Metab.* **13,** 260–273
3. Ding, J., Reynolds, L. M., Zeller, T., Müller, C., Lohman, K., Nicklas, B. J., Kritchevsky, S. B., Huang, Z., de la Fuente, A., Soranzo, N., Settlage, R. E., Chuang, C.-C., Howard, T., Xu, N., Goodarzi, M. O., *et al.* (2015) Alterations of a cellular cholesterol metabolism network are a molecular feature of obesity-related type 2 diabetes and cardiovascular disease. *Diabetes* **64,** 3464–3474
4. Buchovecky, C. M., Turley, S. D., Brown, H. M., Kyle, S. M., McDonald, J. G., Liu, B., Pieper, A. A., Huang, W., Katz, D. M., Russell, D. W., Shendure, J., and Justice, M. J. (2013) A suppressor screen in Mecp2 mutant mice implicates cholesterol metabolism in Rett syndrome. *Nat. Genet.* **45,** 1013–1020
5. Stopsack, K. H., Gerke, T. A., Sinnott, J. A., Penney, K. L., Tyekucheva, S., Sesso, H. D., Andersson, S. O., Andrén, O., Cerhan, J. R., Giovannucci, E. L., Mucci, L. A., and Rider, J. R. (2016) Cholesterol metabolism and prostate cancer lethality. *Cancer Res.* **76,** 4785–4790
6. Brown, D. N., Caffa, I., Cirmena, G., Piras, D., Garuti, A., Gallo, M., Alberti, S., Nencioni, A., Ballestrero, A., and Zoppoli, G. (2016) Squalene epoxidase is a bona fide oncogene by amplification with clinical relevance in breast cancer. *Sci. Rep.* **6,** 19435
7. Varshavsky, A. (1991) Naming a targeting signal. *Cell* **64,** 13–15
8. Howe, V., Chua, N. K., Stevenson, J., and Brown, A. J. (2015) The regulatory domain of squalene monooxygenase contains a re-entrant loop and senses cholesterol via a conformational change. *J. Biol. Chem.* **290,** 27533–27544
9. Zelcer, N., Sharpe, L. J., Loregger, A., Kristiana, I., Cook, E. C., Phan, L., Stevenson, J., and Brown, A. J. (2014) The E3 ubiquitin ligase MARCH6 degrades squalene monooxygenase and affects 3-hydroxy-3-methyl-glutaryl coenzyme A reductase and the cholesterol synthesis pathway. *Mol. Cell. Biol.* **34,** 1262–1270
10. Foresti, O., Ruggiano, A., Hannibal-Bach, H. K., Ejsing, C. S., and Carvalho, P. (2013) Sterol homeostasis requires regulated degradation of squalene monooxygenase by the ubiquitin ligase Doa10/Teb4. *Elife* **2,** e00953
11. Ravid, T., Kreft, S. G., and Hochstrasser, M. (2006) Membrane and soluble substrates of the Doa10 ubiquitin ligase are degraded by distinct pathways. *EMBO J.* **25,** 533–543
12. Johnson, P. R., Swanson, R., Rakhilina, L., and Hochstrasser, M. (1998) Degradation signal masking by heterodimerization of MATα2 and MATa1 blocks their mutual destruction by the ubiquitin–proteasome pathway. *Cell* **94,** 217–227
13. Huyer, G., Piluek, W. F., Fansler, Z., Kreft, S. G., Hochstrasser, M., Brodsky, J. L., and Michaelis, S. (2004) Distinct machinery is required in *Saccharomyces cerevisiae* for the endoplasmic reticulum-associated degradation of a multispanning membrane protein and a soluble luminal protein. *J. Biol. Chem.* **279,** 38369–38378
14. Swanson, R., Locher, M., and Hochstrasser, M. (2001) A conserved ubiquitin ligase of the nuclear envelope/endoplasmic reticulum that functions

in both ER-associated and Matα2 repressor degradation. *Genes Dev.* **15,** 2660–2674
15. Ravid, T., and Hochstrasser, M. (2008) Diversity of degradation signals in the ubiquitin–proteasome system. *Nat. Rev. Mol. Cell Biol.* **9,** 679–690
16. Arteaga, M. F., Wang, L., Ravid, T., Hochstrasser, M., and Canessa, C. M. (2006) An amphipathic helix targets serum and glucocorticoid-induced kinase 1 to the endoplasmic reticulum-associated ubiquitin-conjugation machinery. *Proc. Natl. Acad. Sci. U.S.A.* **103,** 11178–11183
17. Furth, N., Gertman, O., Shiber, A., Alfassy, O. S., Cohen, I., Rosenberg, M. M., Doron, N. K., Friedler, A., Ravid, T. (2011) Exposure of bipartite hydrophobic signal triggers nuclear quality control of Ndc10 at the endoplasmic reticulum/nuclear envelope. *Mol. Biol. Cell.* **22,** 4726–4739
18. Melo, S. P., Barbour, K. W., and Berger, F. G. (2011) Cooperation between an intrinsically disordered region and a helical segment is required for ubiquitin-independent degradation by the proteasome. *J. Biol. Chem.* **286,** 36559–36567
19. Smith, N., Wei, W., Zhao, M., Qin, X., Seravalli, J., Kim, H., and Lee, J. (2016) Cadmium and secondary structure-dependent function of a degron in the Pca1p cadmium exporter. *J. Biol. Chem.* **291,** 12420–12431
20. Guharoy, M., Bhowmick, P., Sallam, M., and Tompa, P. (2016) Tripartite degrons confer diversity and specificity on regulated protein degradation in the ubiquitin–proteasome system. *Nat. Commun.* **7,** 10239
21. Guharoy, M., Bhowmick, P., and Tompa, P. (2016) Design principles involving protein disorder facilitate specific substrate selection and degradation by the ubiquitin–proteasome system. *J. Biol. Chem.* **291,** 6723–6731
22. Fishbain, S., Inobe, T., Israeli, E., Chavali, S., Yu, H., Kago, G., Babu, M. M., and Matouschek, A. (2015) Sequence composition of disordered regions fine-tunes protein half-life. *Nat. Struct. Mol. Biol.* **22,** 214–221
23. Radhakrishnan, A., Ikeda, Y., Kwon, H. J., Brown, M. S., and Goldstein, J. L. (2007) Sterol-regulated transport of SREBPs from endoplasmic reticulum to Golgi: oxysterols block transport by binding to Insig. *Proc. Natl. Acad. Sci. U.S.A.* **104,** 6511–6518
24. Zhang, Y., Motamed, M., Seemann, J., Brown, M. S., and Goldstein, J. L. (2013) Point mutation in luminal loop 7 of Scap protein blocks interaction with loop 1 and abolishes movement to Golgi. *J. Biol. Chem.* **288,** 14059–14067
25. Wang, M. L., Motamed, M., Infante, R. E., Abi-Mosleh, L., Kwon, H. J., Brown, M. S., and Goldstein, J. L. (2010) Identification of surface residues on Niemann-Pick C2 essential for hydrophobic handoff of cholesterol to NPC1 in lysosomes. *Cell Metab.* **12,** 166–173
26. Forman-Kay, J. D., and Mittag, T. (2013) From sequence and forces to structure, function, and evolution of intrinsically disordered proteins. *Structure* **21,** 1492–1499
27. Drin, G., and Antonny, B. (2010) Amphipathic helices and membrane curvature. *FEBS Lett.* **584,** 1840–1847
28. Hubbard, S. R., Hendrickson, W. A., Lambright, D. G., and Boxer, S. G. (1990) X-ray crystal structure of a recombinant human myoglobin mutant at 2.8 A resolution. *J. Mol. Biol.* **213,** 215–218
29. Kendrew, J. C., Bodo, G., Dintzis, H. M., Parrish, R. G., Wyckoff, H., and Phillips, D. C. (1958) A three-dimensional model of the myoglobin molecule obtained by x-ray analysis. *Nature* **181,** 662–666
30. Hung, W.-C., Lee, M.-T., Chen, F.-Y., and Huang, H. W. (2007) The condensing effect of cholesterol in lipid bilayers. *Biophys. J.* **92,** 3960–3967
31. Taylor, M. S., Ruch, T. R., Hsiao, P.-Y., Hwang, Y., Zhang, P., Dai, L., Huang, C. R., Berndsen, C. E., Kim, M.-S., Pandey, A., Wolberger, C., Marmorstein, R., Machamer, C., Boeke, J. D., and Cole, P. A. (2013) Architectural organization of the metabolic regulatory enzyme ghrelin *O*-acyltransferase. *J. Biol. Chem.* **288,** 32211–32228
32. Matevossian, A., and Resh, M. D. (2015) Membrane topology of hedgehog acyltransferase. *J. Biol. Chem.* **290,** 2235–2243
33. Konitsiotis, A. D., Jovanović, B., Ciepla, P., Spitaler, M., Lanyon-Hogg, T., Tate, E. W., and Magee, A. I. (2015) Topological analysis of Hedgehog acyltransferase, a multi-palmitoylated transmembrane protein. *J. Biol. Chem.* **290,** 3293–3307
34. Waldo, G. S., Standish, B. M., Berendzen, J., and Terwilliger, T. C. (1999) Rapid protein-folding assay using green fluorescent protein. *Nat. Biotechnol.* **17,** 691–695
35. Halbleib, K., Pesek, K., Covino, R., Hofbauer, H. F., Wunnicke, D., Hänelt, I., Hummer, G., and Ernst, R. (2017) Activation of the unfolded protein response by lipid bilayer stress. *Mol. Cell* **67,** 673–684
36. Holthuis, J. C., and Menon, A. K. (2014) Lipid landscapes and pipelines in membrane homeostasis. *Nature* **510,** 48–57
37. Giang, H., and Schick, M. (2014) How cholesterol could be drawn to the cytoplasmic leaf of the plasma membrane by phosphatidylethanolamine. *Biophys. J.* **107,** 2337–2344
38. Tanaka, H., Takahashi, T., Xie, Y., Minami, R., Yanagi, Y., Hayashishita, M., Suzuki, R., Yokota, N., Shimada, M., Mizushima, T., Kuwabara, N., Kato, R., and Kawahara, H. (2016) A conserved island of BAG6/Scythe is related to ubiquitin domains and participates in short hydrophobicity recognition. *FEBS J.* **283,** 662–677
39. Gilon, T., Chomsky, O., and Kulka, R. G. (2000) Degradation signals recognized by the Ubc6p-Ubc7p ubiquitin-conjugating enzyme pair. *Mol. Cell. Biol.* **20,** 7214–7219
40. Fredrickson, E. K., Rosenbaum, J. C., Locke, M. N., Milac, T. I., and Gardner, R. G. (2011) Exposed hydrophobicity is a key determinant of nuclear quality control degradation. *Mol. Biol. Cell.* **22,** 2384–2395
41. Sanchis, J., Fernández, L., Carballeira, J. D., Drone, J., Gumulya, Y., Höbenreich, H., Kahakeaw, D., Kille, S., Lohmer, R., Peyralans, J. J., Podtetenieff, J., Prasad, S., Soni, P., Taglieber, A., Wu, S., *et al.* (2008) Improved PCR method for the creation of saturation mutagenesis libraries in directed evolution: application to difficult-to-amplify templates. *Appl. Microbiol. Biotechnol.* **81,** 387–397
42. Stevenson, J., Krycer, J. R., Phan, L., and Brown, A. J. (2013) A practical comparison of ligation-independent cloning techniques. *PLoS ONE* **8,** e83888
43. Brown, A. J., Sun, L., Feramisco, J. D., Brown, M. S., and Goldstein, J. L. (2002) Cholesterol addition to ER membranes alters conformation of SCAP, the SREBP escort protein that regulates cholesterol metabolism. *Mol. Cell* **10,** 237–245
44. Zerenturk, E. J., Sharpe, L. J., and Brown, A. J. (2014) DHCR24 associates strongly with the endoplasmic reticulum beyond predicted membrane domains: implications for the activities of this multi-functional enzyme. *Biosci. Rep.* 34, e00098
45. Xu, D., and Zhang, Y. (2012) *Ab initio* protein structure assembly using continuous structure fragments and optimized knowledge-based force field. *Proteins* **80,** 1715–1735
46. Van Der Spoel, D., Lindahl, E., Hess, B., Groenhof, G., Mark, A. E., and Berendsen, H. J. (2005) GROMACS: fast, flexible, and free. *J. Comput. Chem.* **26,** 1701–1718
47. Jorgensen, W. L., Maxwell, D. S., and Tirado-Rives, J. (1996) Development and testing of the OPLS all-atom force field on conformational energetics and properties of organic liquids. *J. Am. Chem. Soc.* **118,** 11225–11236
48. Jorgensen, W. L., Chandrasekhar, J., Madura, J. D., Impey, R. W., and Klein, M. L. (1983) Comparison of simple potential functions for simulating liquid water. *J. Chem. Phys.* **79,** 926–935
49. Darden, T., York, D., and Pedersen, L. (1993) Particle mesh Ewald: an N·log(N) method for Ewald sums in large systems. *J. Chem. Phys.* **98,** 10089–10092
50. Bussi, G., Donadio, D., and Parrinello, M. (2007) Canonical sampling through velocity rescaling. *J. Chem. Phys.* **126,** 14101
51. Parrinello, M., and Rahman, A. (1981) Polymorphic transitions in single crystals: a new molecular dynamics method. *J. Appl. Phys.* **52,** 7182–7190
52. Kearse, M., Moir, R., Wilson, A., Stones-Havas, S., Cheung, M., Sturrock, S., Buxton, S., Cooper, A., Markowitz, S., Duran, C., Thierer, T., Ashton, B., Meintjes, P., and Drummond, A. (2012) Geneious Basic: an integrated and extendable desktop software platform for the organization and analysis of sequence data. *Bioinformatics* **28,** 1647–1649
53. Buchan, D. W., Minneci, F., Nugent, T. C., Bryson, K., and Jones, D. T. (2013) Scalable web services for the PSIPRED protein analysis workbench. *Nucleic Acids Res.* **41,** W349–W357
54. Lamiable, A., Thévenet, P., Rey, J., Vavrusa, M., Derreumaux, P., and Tufféry, P. (2016) PEP-FOLD3: faster *de novo* structure prediction for linear peptides in solution and in complex. *Nucleic Acids Res.* **44,** W449–W454

55. Gautier, R., Douguet, D., Antonny, B., and Drin, G. (2008) HELIQUEST: a web server to screen sequences with specific α-helical properties. *Bioinformatics* **24,** 2101–2102
56. Linding, R., Jensen, L. J., Diella, F., Bork, P., Gibson, T. J., and Russell, R. B. (2003) Protein disorder prediction: implications for structural proteomics. *Structure* **11,** 1453–1459
57. Jones, D. T., and Cozzetto, D. (2015) DISOPRED3: precise disordered region predictions with annotated protein-binding activity. *Bioinformatics* **31,** 857–863
58. Peng, K., Vucetic, S., Radivojac, P., Brown, C. J., Dunker, A. K, Obradovic, Z. (2005) Optimizing long intrinsic disorder predictors with protein evolutionary information. *J. Bioinform. Comput. Biol.* **3,** 35–60
59. Linding, R., Russell, R. B., Neduva, V., and Gibson, T. J. (2003) GlobPlot: exploring protein sequences for globularity and disorder. *Nucleic Acids Res.* **31,** 3701–3708
60. Dosztányi, Z., Csizmok, V., Tompa, P., and Simon, I. (2005) IUPred: web server for the prediction of intrinsically unstructured regions of proteins based on estimated energy content. *Bioinformatics* **21,** 3433–3434
61. Romero, P., Obradovic, Z., and Dunker, A. (1997) Sequence data analysis for long disordered regions prediction in the calcineurin family. *Genome Inform. Ser. Workshop Genome Inform.* **8,** 110–124
62. Li, X., Romero, P., Rani, M., Dunker, A. K., and Obradovic, Z. (1999) Predicting protein disorder for N-, C-, and internal regions. *Genome Inform. Ser. Workshop Genome Inform.* **10,** 30–40
63. Garner, E., Romero, P., Dunker, A. K., Brown, C., and Obradovic, Z. (1999) Predicting binding regions within disordered proteins. *Genome Inform. Ser. Workshop Genome Inform.* **10,** 41–50
64. Ishida, T., and Kinoshita, K. (2007) PrDOS: Prediction of disordered protein regions from amino acid sequence. *Nucleic Acids Res.* 35, W460–W464
65. Garcia-Boronat, M., Diez-Rivero, C. M., Reinherz, E. L., and Reche, P. A. (2008) PVS: a web server for protein sequence variability analysis tuned to facilitate conserved epitope discovery. *Nucleic Acids Res.* **36,** W35–W41
66. Wu, T. T., and Kabat, E. A. (1970) An analysis of the sequences of the variable regions of Bence Jones proteins and myeloma light chains and their implications for antibody complementarity. *J. Exp. Med.* **132,** 211–250